

Building Subtraction Operators and Controllers via Molecular Sequestration

Christian Cuba Samaniego[®], Yili Qian, Katelyn Carleton, and Elisa Franco[®]

Abstract—We show how subtraction can be performed via a simple chemical reaction network that includes molecular sequestration. The network computes the difference between the production rate parameters of the two mutually sequestering species. We benefit from introducing a simple change of variables, that facilitates the derivation of an approximate solution for the differential equations modeling the chemical reaction network, under a time scale separation assumption that is valid when the sequestration rate parameter is sufficiently fast. Our main result is that we provide simple expressions confirming that temporal subtraction occurs when the inputs are constant or time varying. Through simulations, we discuss two sequestration-based architectures for feedback control in light of the subtraction operations they perform.

Index Terms—Molecular sequestration, chemical reactions, molecular controllers, biological systems.

I. INTRODUCTION

OLECULAR sequestration (titration) is a prevalent mechanism in biology that consists of the stoichiometric binding of two species. Sequestration can involve many classes of molecules; examples include RNA-RNA binding, transcription factors binding to promoters, enzymes and their substrates, receptors and their ligands, or antibodies and antigens. This binding process plays a crucial role in various biological processes, including signal transduction, regulation of gene expression, immune response, and metabolic pathways. Is there an underlying operation being computed by molecular sequestration, that is key to enable a broad variety of functions? This question is difficult to answer in the native context of the cell, but there is evidence that sequestration enables the computation of the difference in the level of participating molecules [1], [2]. In synthetic biology, mathematical

Manuscript received 21 April 2023; revised 20 June 2023; accepted 27 June 2023. Date of publication 12 July 2023; date of current version 20 November 2023. This work was supported in part by BBRSC-NSF/BIO under Award 2020039, and in part by NSF CCF/SHF under Award 2107483 to EF. Recommended by Senior Editor F. Dabbene. (Christian Cuba Samaniego, Yili Qian, and Katelyn Carleton contributed equally to this work.) (Corresponding author: Elisa Franco.)

Christian Cuba Samaniego, Katelyn Carleton, and Elisa Franco are with the Department of Mechanical and Aerospace Engineering, University of California at Los Angeles, Los Angeles, CA 90095 USA (e-mail: ccubasam@g.ucla.edu; efranco@seas.ucla.edu).

Yili Qian is with the Department of Biochemistry, University of Wisconsin-Madison, Madison, WI 53706 USA (e-mail: qian9@wisc.edu).

Digital Object Identifier 10.1109/LCSYS.2023.3294690

modeling has shown how to leverage this property to build molecular controllers [2], [3], [4], [5], [6], networks for frequency modulation [7], bistable switches with tunable hysteresis [8], [9], gradient detectors [10], [11], and biomolecular perceptrons [12]; some of these ideas have been experimentally demonstrated [13], [14], [15], [16], [17], [18]. It is abundantly evident that sequestration helps compute the difference of two inputs at steady-state [1], [2], [3], [4], [17], and linear analysis shows that it works as a sum junction [19]. However, a complete analysis of the dynamical behavior of these sequestration reactions is still missing, making it challenging to understand/design its behavior when the inputs are time-varying and in the presence of dilution/degradation of the reactants.

Another limitation that needs to be addressed is the fact that sequestration can only calculate the *positive part of a subtraction operation*, due to the biological nature of the participating components [20]. In this sense, it bears similarity to functions computing an absolute value [7].

Here we provide a complete temporal analysis of a molecular sequestration network, modeled through ordinary differential equations, and we show that it can compute differences in the presence of dilution/degradation, both transiently and at steady state. To come to this conclusion, we introduce a change of variables that makes it easier to apply time scale separation arguments, which decouples the system into a linear and non-linear part. This allows us to find an approximate solution of the output of this network, which is proportional to the difference of the molecular inputs, whether they are constant or time varying. We then discuss how sequestration can be used as a low-pass controller within biomolecular feedback loops. Through simulation we also show how low-pass controllers in a "dual rail" architecture improves the response speed of a feedback circuit tracking time-varying inputs. We expect that our modeling results will boost the use of sequestration within complex synthetic biological networks, and that they will facilitate the formulation of hypotheses about the roles of sequestration in natural systems.

II. A MODEL FOR MOLECULAR SEQUESTRATION AND ITS SINGULAR PERTURBATION FORM

Our chemical network for subtraction includes two species, X and Y, that mutually sequester and bind to form a complex C (Fig. 1). We assume that X and Y have zero-order time-varying production rates $\alpha(\tau)$ and $\beta(\tau)$. We model dilution/degradation as a first-order process with rate parameter ϕ ,

2475-1456 © 2023 IEEE. Personal use is permitted, but republication/redistribution requires IEEE permission. See https://www.ieee.org/publications/rights/index.html for more information.

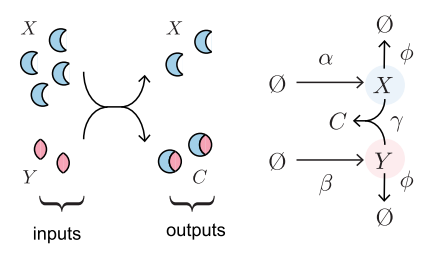


Fig. 1. Schematic of the reactions occurring in the molecular sequestration network considered here.

assumed to be the same for simplicity. The sequestration of X and Y happens with a constant rate parameter γ . We postulate that γ can be rescaled [3], [5]. The chemical reactions are:

$$\emptyset \xrightarrow{\alpha(\tau)} X \quad \emptyset \xrightarrow{\beta(\tau)} Y \text{ Production}$$

$$X \xrightarrow{\phi} \emptyset \quad Y \xrightarrow{\phi} \emptyset \text{ Decay}$$

$$X + Y \xrightarrow{\gamma} C \quad C \xrightarrow{\phi} \emptyset \text{ Sequestration/Decay.}$$
 (1)

From the reactions in (1), we derive an Ordinary Differential Equation (ODE) model using the law of mass action:

$$\dot{x}(\tau) = \alpha(\tau) - \gamma x(\tau) y(\tau) - \phi x(\tau)
\dot{y}(\tau) = \beta(\tau) - \gamma x(\tau) y(\tau) - \phi y(\tau)
\dot{c}(\tau) = \gamma x(\tau) y(\tau) - \phi c(\tau),$$
(2)

where the \dot{x} , \dot{y} , and \dot{c} indicate derivatives with respect to the time variable τ . Previous work considering similar reactions assumed (i) $\phi = 0$ and (ii) $\alpha(\tau) > \beta(\tau)$ for all time [2].

When $\alpha = \beta = 0$, we can immediately provide intuition as to why molecular sequestration realizes a subtraction operator. First, sequestration implies there is a 1:1 binding ratio between X and Y (one molecule of X binds to one molecule of Y). Then, in the limit case where $\phi \to 0$, the final concentration of the non-limiting species is the difference between the initial concentrations of the sequestering species [1]. Suppose x(0) > 0y(0): the final concentration of X (non-limiting species) will be equal to the difference in the initial concentrations x(0) – y(0), given that all free Y (the limiting species) is bound into the complex C. In practice, however, matters are made more complex due to the presence of time varying input functions $\alpha(\tau)$ and $\beta(\tau)$, and of degradation and dilution, scaled by parameter ϕ . Next, we illustrate how to examine this case by introducing an approximation valid for constant and timechanging inputs, which we assume to be bounded and nonnegative.

Assumption 1: There exist positive constants α^* , β^* such that $0 \le \alpha(\tau) \le \alpha^*$ and $0 \le \beta(\tau) \le \beta^*$ for all $t \ge 0$.

We do not introduce requirements on the relative magnitude of the inputs.

To obtain a non-dimensional model, we first rescale time as $t = \phi \tau$, and define new states variables $\hat{x} = (\frac{\phi}{m})x$, $\hat{y} = (\frac{\phi}{m})y$, $\hat{c} = (\frac{\phi}{m})c$, and new rates $\hat{\alpha}(t) = \frac{\alpha(t/\phi)}{\phi m}$, $\hat{\beta}(t) = \frac{\beta(t/\phi)}{\phi m}$ and $\hat{\gamma} = \frac{m}{\phi^2} \gamma$, where $m = \max(\alpha^*, \beta^*)$. Our non-dimensional model is now:

$$\dot{\hat{x}} = \hat{\alpha}(t) - \hat{\gamma}\hat{x}\hat{y} - \hat{x},
\dot{\hat{y}} = \hat{\beta}(t) - \hat{\gamma}\hat{x}\hat{y} - \hat{y},
\dot{\hat{c}} = \hat{\gamma}\hat{x}\hat{y} - \hat{c}.$$
(3)

Next, we apply a coordinate transformation that makes it possible to put the system in its singular perturbation form. We begin by applying a coordinate transformation:

$$\hat{x}^T = \hat{x} + \hat{c}, \ \hat{y}^T = \hat{y} + \hat{c}.$$
 (4)

The new variables \hat{x}^T and \hat{y}^T represent the total concentration of species X and Y, which includes molecules that are free or bound to make the complex C, and system (3) becomes:

$$\dot{\hat{x}}^T = \hat{\alpha}(t) - \hat{x}^T,
\dot{\hat{y}}^T = \hat{\beta}(t) - \hat{y}^T,
\dot{\hat{c}} = \hat{\gamma}(\hat{x}^T - \hat{c})(\hat{y}^T - \hat{c}) - \hat{c}.$$
(5)

Let $\xi := 1/\hat{\gamma}$, system (5) can be put into a singular perturbation form:

$$\dot{\hat{x}}^T = \hat{\alpha}(t) - \hat{x}^T,
\dot{\hat{y}}^T = \hat{\beta}(t) - \hat{y}^T,
\xi \dot{\hat{c}} = (\hat{x}^T - \hat{c})(\hat{y}^T - \hat{c}) - \xi \hat{c}.$$
(6)

Note that the first two equations of system (6) are linear and do not depend on ξ . In the next sections, we use the transformed system (6) to demonstrate its capacity to perform a subtraction operation.

III. THE MOLECULAR SEQUESTRATION NETWORK PERFORMS A SUBTRACTION OPERATION

We will show that the solution \hat{x} of system (3) satisfies:

$$\lim_{\xi \to 0^+} \hat{x}(t) = \hat{x}_p(t) \triangleq \max[0, (\hat{x}^T - \hat{y}^T)].$$
 (7)

In other words, $\hat{x}(t)$ can be approximated by \hat{x}_p , the nonnegative part of the subtraction of variables \hat{x}^T and \hat{y}^T that capture the total amounts of molecules \hat{x} and \hat{y} . It is also possible to prove that $\lim_{\xi \to 0^+} \hat{y}(t) = \hat{y}_p(t) \triangleq \max \left[0, (\hat{y}^T - \hat{x}^T)\right]$ with a similar approach. For the sake of brevity, we will focus exclusively on demonstrating (7). Note that for $\xi \to 0^+$, the dynamics of \hat{c} in (6) evolve on a fast timescale. In particular, let $\tau = t/\xi$ be the fast timescale, then we have $d\hat{c}/d\tau = (\hat{x}^T - \hat{c})(\hat{y}^T - \hat{c}) - \xi\hat{c}$, which has two equilibria that are $\mathcal{O}(\xi)$ close to \hat{x}^T and \hat{y}^T . In the following, we will prove this formally and show that $\hat{c}(t)$ approaches the minimum of $\hat{x}^T(t)$ and $\hat{y}^T(t)$:

$$\lim_{\varepsilon \to 0^+} \hat{c}(t) = \Gamma(\hat{x}^T, \hat{y}^T) \triangleq \min\left[\hat{x}^T(t), \hat{y}^T(t)\right]. \tag{8}$$

For this purpose, we define

$$e(t) \triangleq \Gamma(\hat{\mathbf{x}}^T, \hat{\mathbf{y}}^T) - \hat{c}(t) \tag{9}$$

and aim to find an upper bound for |e(t)|.

Lemma 1: The dynamics of the error (9) satisfy $e(t) \ge 0$ for all $t \ge 0$.

Proof: The dynamics of (3) is positively invariant in the nonnegative orthant $\mathbb{R}^3_{\geq 0}$. Since $\hat{x}^T(t) - \hat{c}(t) = \hat{x}(t) \geq 0$ and $\hat{y}^T(t) - \hat{c}(t) = \hat{y}(t) \geq 0$, we have $e(t) = \Gamma(t) - \hat{c}(t) = \min(\hat{x}^T, \hat{y}^T) - \hat{c}(t) \geq 0$.

The error dynamics can be written as:

$$D^{+}e = D^{+}\Gamma - \frac{1}{\xi}(\hat{x}^{T} - \Gamma + e)(\hat{y}^{T} - \Gamma + e) + (\Gamma - e),$$

= $D^{+}\Gamma - \frac{1}{\xi}e(\Lambda - \Gamma + e) + (\Gamma - e)$ (10)

where D^+ indicates right-hand derivative with respect to time and $\Lambda(\hat{x}^T, \hat{y}^T) \triangleq \max(\hat{x}^T, \hat{y}^T)$. We will first show that, as a consequence of Assumption 1, the derivative $D^+\Gamma$ is bounded.

Lemma 2: Suppose that the initial conditions are such that $\hat{x}^T(0) \leq \bar{\alpha}$ and $\hat{y}^T(0) \leq \bar{\beta}$, then there exist positive constants M and $\bar{\Gamma}$, independent of ξ , such that $|D^+\Gamma(\hat{x}^T,\hat{y}^T)| \leq M$ and $0 \leq \Gamma \leq \bar{\Gamma}$ for all $t \geq 0$.

Proof: Consider the dynamics of the slow variables (\hat{x}^T, \hat{y}^T) in (6): $\hat{x}^T = \hat{\alpha}(t) - \hat{x}^T$, $\hat{y}^T = \hat{\beta}(t) - \hat{y}^T$. Given Assumption 1, let $\bar{\alpha}$ and $\bar{\beta}$ be the upper bounds for $\hat{\alpha}(t)$ and $\hat{\beta}(t)$, respectively. By the comparison principle, we have $0 \le \hat{x}^T(t) \le \bar{\alpha}$ and $0 \le \hat{y}^T(t) \le \bar{\beta}$ for all $t \ge 0$. Hence, we have $\hat{x}^T \in [-\bar{\alpha}, \bar{\alpha}]$ and $\hat{y}^T \in [-\bar{\beta}, \bar{\beta}]$. For this reason, there exists an ξ -independent constant M such that $|\hat{x}^T(t)|, |\hat{y}^T(t)| \le M/2$ for all $t \ge 0$. Because $\Gamma(\hat{x}^T, \hat{y}^T) = \min(\hat{x}^T, \hat{y}^T)$, we have $|D^+\Gamma(\hat{x}^T, \hat{y}^T)| \le |\hat{x}^T(t)| + |\hat{y}^T(t)| = M$. The bound on $\Gamma(t)$ is a trivial consequence of Assumption 1.

The assumptions on initial conditions $\hat{x}^T(0)$ and $\hat{y}^T(0)$ are for technical convenience and could be relaxed as the set $[0, \bar{\alpha}] \times [0, \bar{\beta}]$ is globally attractive for (\hat{x}^T, \hat{y}^T) . We will now use comparison principle [21] to develop bounds for the error dynamics (10):

$$D^{+}e = D^{+}\Gamma - \frac{1}{\xi}(\Lambda - \Gamma)e - \frac{e^{2}}{\xi} + \Gamma - e$$

$$\leq B - \frac{1}{\xi}e^{2} - \frac{1}{\xi}\Delta(t)e, \tag{11}$$

where we applied the results in Lemma 2, and $B \triangleq M + \bar{\Gamma} > 0$ and $\Delta(t) \triangleq \max(\hat{x}^T, \hat{y}^T) - \min(\hat{x}^T, \hat{y}^T)$ are both ξ -independent. The following Theorem states that, pick any T > 0 such that $\Delta(t)$ is bounded below by some ξ -independent constant for all $t \leq T$, there exists a sufficiently small ξ such that $|e(t)| \leq \mathcal{O}(\sqrt{\xi})$ for all $t \geq T$.

Theorem 1: Under Assumption 1 and suppose that there exist ξ -independent constants $T, \delta > 0$ such that $\Delta(t) = \max(\hat{x}^T, \hat{y}^T) - \min(\hat{x}^T, \hat{y}^T) \geq \delta$ for all $0 \leq t \leq T$. Then there exist positive constants ξ^* and p, such that

$$|e(t)| \le \sqrt{p\xi}, \quad \forall t \ge T, \quad \forall 0 < \xi < \xi^*.$$
 (12)

Proof: The proof consists of two parts. First, we show that for any p > B the set $\Omega \triangleq [0, \sqrt{p\xi}]$ is positively invariant. This is because, by (11) and Lemma 1, for any $e \geq p$, we have $D^+e \leq B - e^2/\xi \leq B - p^2/\xi < 0$. Hence, the set Ω is positively invariant. Next, we show that the set Ω is attractive, and for any $e(0) \notin \Omega$, there exists sufficiently small ξ for e(t) to enter Ω in any chosen T. By inequality (11), we have

$$D^{+}e \le B - \frac{1}{\xi}\Delta(t)e \le B - \frac{\delta}{\xi}e, \ \forall t \le T.$$
 (13)

By (13) and the comparison principle [21], we have

$$e(t) \le \xi \frac{B}{\delta} (1 - \exp(-\delta t/\xi)) + e_0 \exp(-\delta t/\xi),$$

 $\forall t < T, e_0 \triangleq e(0).$

Hence $e(T) \leq \xi B/\delta + e_0 \exp(-\delta T/\xi) \leq 2\xi B/\delta$, if $g(\xi) \triangleq \xi \ln\left(\frac{\delta e_0}{2B\xi}\right) \leq T\delta$. Since $\lim_{\xi \to 0^+} g(\xi) = 0$ and $dg/d\xi(\xi) > 0$ for sufficiently small ξ , there exists an ξ^* such that $g(\xi) \leq T\delta$ for all $0 < \xi \leq \xi^*$. Therefore, $e(T) \in \Omega$ for any $\xi \leq \min\left(\frac{p\delta^2}{4B^2}, \xi^*\right)$. This completes the proof, as we showed that

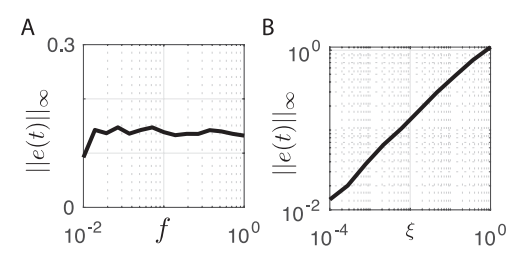


Fig. 2. **Error Analysis** (A) The magnitude of the error $e(t) = \min(\hat{x}^T, \hat{y}^T) - \hat{c}$ is plotted as a function of input frequency, f. The simulation is carried out using the setting described in Remark 1 and ξ is kept constant at 0.01. The error is largely independent of the input frequency. (B) the error magnitude is plotted as a function of ξ . The simulation is carried out using the setting described in Remark 1 and input frequency is kept constant at 0.1.

e(t) enters the positively invariant set Ω of size $\mathcal{O}(\sqrt{\xi})$ at t = T for sufficiently small ξ .

Because we have shown that e(t) converges to zero when $\xi \to 0^+$, then expression (8) holds and so does our initial equation (7).

Remark 1: Note that the error bound is independent of the derivative of the inputs $\dot{\hat{\alpha}}(t)$ and $\dot{\hat{\beta}}(t)$. This is supported by the simulation in Fig. 2, where we varied the frequencies of the input sinusoidal signals but the error magnitude remains roughly constant. The simulation in Figure 2 shows that $\mathcal{O}(\sqrt{\xi})$ is a tight upper bound of the error dynamics. Simulations are carried out with $\hat{\alpha}(t) = 1.2 \cdot (1.1 + \sin(f \cdot t))$ and $\hat{\beta}(t) = 1.5 \cdot (1.1 + \cos(f \cdot t))$.

Remark 2: If the complex C dissociates back into reactants X and Y with reaction parameter γ^- , the error analysis becomes perturbed by an additional term of order $\mathcal{O}(\xi)$, which is negligible given the $\mathcal{O}(\sqrt{\xi})$ upper bound in Theorem 1.

Remark 3: With different degradation constants for x, y and c, equations (6) become coupled, and the analysis above cannot be easily adapted to consider this case. Computational simulations (not shown) suggest that a large discrepancy among degradation rates can deteriorate the subtraction computation.

IV. LINEAR APPROXIMATION AND COMPUTATIONAL SOLUTION OF THE SUBTRACTION NETWORK

Building on the result of the previous section we can introduce a linear approximation to the dynamics of the molecular sequestration network (2). The approximation holds for $\xi \to 0^+$. We now consider dimensional equations; we take the derivative of the right side of equation (7) and substituting the definition of $\dot{x}^T(\tau)$ and $\dot{y}^T(\tau)$, we find:

$$\dot{x}_p(\tau) = \begin{cases} \alpha(\tau) - \beta(\tau) - \phi x_p(\tau), & x^T(\tau) \ge y^T(\tau), \\ 0, & x^T(\tau) < y^T(\tau). \end{cases}$$
(14)

Similarly, we can derive the approximation for \hat{y} :

$$\dot{y}_p(\tau) = \begin{cases} 0, & x^T(\tau) \ge y^T(\tau), \\ \beta(\tau) - \alpha(\tau) - \phi y_p(\tau), & x^T(\tau) < y^T(\tau). \end{cases}$$

These piecewise linear ODEs include two species whose dynamics are decoupled and can be solved exactly and independently. We can also map these ODEs to an "equivalent" chemical reaction network sketched in Fig. 3. When α and β are constant, the dynamics of x^T and y^T are linear (see also the

$$\begin{array}{ccccc}
A & \emptyset & B & \emptyset \\
\emptyset & \xrightarrow{\alpha} & \uparrow^{\phi} & & & & & & & & & & & & & \\
\emptyset & \xrightarrow{\alpha} & \uparrow^{\phi} & & & & & & & & & & & \\
\emptyset & \xrightarrow{\alpha} & \chi & & & & & & & & & & & \\
C & \swarrow & \gamma & & & & & & & & & & \\
\emptyset & \xrightarrow{\gamma} & \chi_{p} & & & & & & & & & & \\
\emptyset & \xrightarrow{\gamma} & \chi_{p} & & & & & & & & & & \\
\emptyset & \xrightarrow{\beta} & \chi_{p} & & & & & & & & & & \\
\downarrow^{\alpha} & \downarrow^{\phi} & & & & & & & & & & \\
\downarrow^{\alpha} & \downarrow^{\phi} & & & & & & & & & & \\
\downarrow^{\alpha} & \downarrow^{\phi} & & & & & & & & & \\
\downarrow^{\alpha} & \downarrow^{\phi} & & & & & & & & & \\
\downarrow^{\alpha} & \downarrow^{\phi} & & & & & & & & \\
\downarrow^{\alpha} & \downarrow^{\phi} & & & & & & & & \\
\downarrow^{\alpha} & \downarrow^{\phi} & & & & & & & \\
\downarrow^{\alpha} & \downarrow^{\phi} & & & & & & & \\
\downarrow^{\alpha} & \downarrow^{\phi} & & & & & & & \\
\downarrow^{\alpha} & \downarrow^{\phi} & & & & & & \\
\downarrow^{\alpha} & \downarrow^{\phi} & & & & & & \\
\downarrow^{\alpha} & \downarrow^{\phi} & & & & & & \\
\downarrow^{\alpha} & \downarrow^{\phi} & & & & & & \\
\downarrow^{\alpha} & \downarrow^{\phi} & & & & & \\
\downarrow^{\alpha} & \downarrow^{\phi} & & & & & \\
\downarrow^{\alpha} & \downarrow^{\phi} & & & & & \\
\downarrow^{\alpha} & \downarrow^{\phi} & & & & & \\
\downarrow^{\alpha} & \downarrow^{\phi} & & & \\
\downarrow^{\alpha} & \downarrow^{\alpha} & & \\$$

Fig. 3. **Equivalent chemical reactions** (A) The original sequestration network. (B) The equivalent reactions corresponding to the approximated dynamics (14).

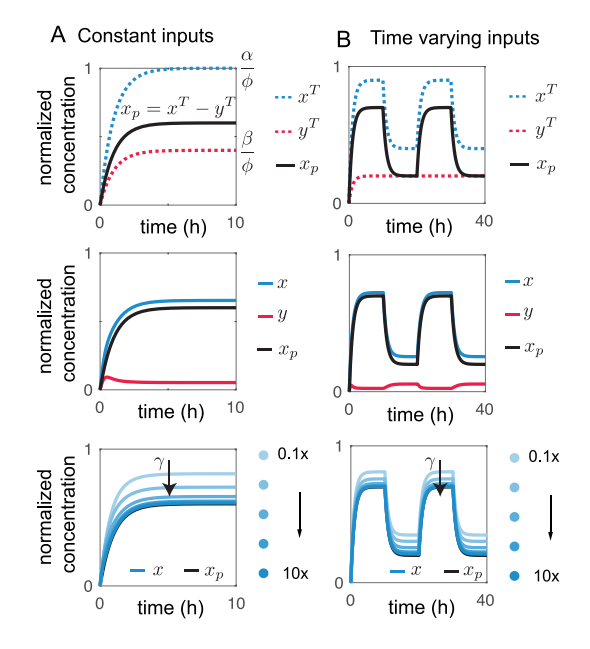


Fig. 4. Approximated solution of molecular sequestration. Behavior of the sequestration operator under (A) a constant inputs $\alpha=1~\mu M/h$ and $\beta=0.4~\mu M/h$ ($\gamma=10/\mu M/h$, and $\phi=1/h$) and (B) a time-varying square wave input where $\alpha(\tau)=0.5~\times~sgn[\sin{(\frac{2\pi t}{20}t+1)}]/2+0.4~\mu M/h$ and $\beta(\tau)=0.2~\mu M/h$. Top panels highlight the definition of $x_p=x^T-y^T$. The center panels compare the approximated dynamics of x_p (black) with the simulated dynamics of x (blue) and y (red). Bottom panels simulated dynamics of x (blue) converging to the approximated dynamics x_p (black) as $y\to\infty$. These simulations integrate equations (2) and the approximation (14).

first two non dimensional equations in model (5)) and $x_p(\tau)$ can be found exactly.

Simulations of the subtraction module are shown in Fig. 4A. Specifically, the bottom panel shows that the solution $x(\tau)$ (blue shades) of the nonlinear model (2) converges to the approximation x_p (black) as $\gamma \to \infty$ ($\xi \to 0$). When the input rates $\alpha(\tau)$ and $\beta(\tau)$ are time varying, equations (14) can be easily integrated to obtain the estimates x_p and y_p without pre-computing x^T and y^T : inequality $x^T(\tau) < y^T(\tau)$ can be replaced by $x_p(\tau) < 0$, and $x^T(\tau) \ge y^T(\tau)$ can be replaced by $x_p(\tau) \ge 0$ (similarly for y and y_p).

We illustrate this with the simulations in Fig. 4B. As a test of time-varying input we take $\alpha(\tau)$ to be a square wave, while input $\beta(\tau)$ is kept constant. The top panel of Fig. 4B reports the trajectories for $x^T = x + c$ (red dotted line), $y^T = y + c$ (blue dotted line), and the approximate trajectory $x_p = x^T - y^T$ (14) (black solid line). The center panel in Fig. 4B compares the trajectories of x (solid blue line) and x_p (solid black line); this plot also shows that y (solid red line) is small but not zero. The bottom panel of Fig. 4B compares the trajectories of x

(solid blue lines) for different values of sequestration constant γ and the ideal trajectory $x_p(\text{solid black line})$: larger γ results in the overlapping of x and x_p . To summarize, for sufficiently large γ (which is equivalent to taking a small ξ) the solution computed for the linear ODEs (14) approaches the full solution of the nonlinear ODEs (6).

V. BUILDING MOLECULAR FEEDBACK CONTROLLERS THROUGH THE SUBTRACTION OPERATOR

Network (2) has been used as a molecular feedback controller [22]. In this context, we re-examine the network by focusing on its capacity to perform a subtraction operation and by taking advantage of the approximations derived earlier. Our goal is to regulate a standard protein production/degradation process, described by these chemical reactions:

$$X_1 \xrightarrow{\alpha_s} Y$$
, $Y \xrightarrow{\phi_s} \varnothing$, Production and Decay of Y ,

where we do not have direct control over α_s and ϕ_s , while we can manipulate the abundance of species X_1 . We want to match the level of the process Y with the level of a reference species R (Fig. 5A and B, gray box).

A low-pass controller (LPC): We begin by applying the analysis described earlier to a leaky molecular sequestration controller [5]: this exercise is useful as it brings out its inherent similarity to a low-pass controller (LPC). We introduce two controller species, X_1 and Z_1 . The reference species R produces X_1 at a rate parameter θ_c ; to close the loop, we use species Y_1 (process output) to induce the production of species Y_2 at a rate parameter Y_2 . The controller species Y_2 and Y_3 sequester each other at a rate parameter Y_2 (forming a complex Y_3), and they decay at rate parameter Y_3 . The reactions are summarized below (blue box in Fig. 5A):

$$R \xrightarrow{\theta_c} X_1$$
 $Y \xrightarrow{\kappa_c} Z_1$ Production $X_1 \xrightarrow{\phi_c} \varnothing$ $Z_1 \xrightarrow{\phi_c} \varnothing$ Decay $X_1 + Z_1 \xrightarrow{\gamma_c} C_1$ Sequestration.

Through the law of mass action, the closed loop model is:

$$\dot{x}_{1} = \theta_{c}r - \gamma_{c}x_{1}z_{1} - \phi_{c}x_{1},
\dot{z}_{1} = \kappa_{c}y - \gamma_{c}x_{1}z_{1} - \phi_{c}z_{1},
\dot{c}_{1} = \gamma_{c}x_{1}z_{1} - \phi_{c}c_{1},
\dot{y} = \alpha_{s}x_{1} - \phi_{s}y.$$
(15)

Our previous analysis $(\gamma \to \infty)$ allows us to derive a simple interpretation of how this controller works. Through a change of variable $x_1^T = x_1 + c_1$, and $z_1^T = z_1 + c_1$ we can find the approximated solution to $x_1(\tau)$:

$$\dot{x}_{1,p}(\tau) = \begin{cases} \theta_c r(\tau) - \kappa_c y(\tau) - \phi_c x_{1,p}(\tau) & x_1^T(\tau) \ge z_1^T(\tau) \\ 0 & x_1^T(\tau) < z_1^T(\tau), \end{cases}$$
(16)

and similarly we can find the dynamics of $z_{1,p}$. By defining the rescaled error $e(\tau) = \frac{\theta_c}{\kappa_c} r(\tau) - y(\tau)$, it is easy to derive the frequency response mapping e to $x_{1,p}$. When $x_1^T(\tau) \ge z_1^T(\tau)$:

$$X_{1,p}(j\omega) = \frac{\kappa_c}{j\omega + \phi_c} E(j\omega) = C_1(j\omega) E(j\omega), \qquad (17)$$

when $x_1^T(\tau) < z_1^T(\tau)$, $X_{1,p}(j\omega) = 0$. In expression (17), $C_1(j\omega)$ is an LPC with DC gain κ_c/ϕ_c and corner frequency ϕ_c . At low frequencies ($\omega \ll \phi_c$), $C_1(j\omega)$ behaves like a proportional controller with gain κ_c/ϕ_c . For $\phi_c \to 0$, i.e., in the absence of dilution/degradation, $C_1(j\omega)$ becomes an integrator $C_1(j\omega) = \kappa_c/j\omega$, which is consistent with dilution-free sequestration controllers [3]. It is known that ideal integral behavior is possible only in the absence of dilution/degradation [5]. In the presence of degradation, the leaky molecular sequestration controller can only achieve quasi-integral action: fast sequestration and large production rate parameters [5], [16], [18], or input-output ultrasensitivity [5], [23] are required to minimize the steady-state error between reference and output.

A dual-rail controller (DRC): It is apparent that the approximated output $x_{1,p}$ of our controller (16) is non-zero only when $x_1^T(\tau) \geq z_1^T(\tau)$, meaning that it only responds to the positive part of the difference between $x_1^T(\tau)$ and $z_1^T(\tau)$. When $x_1^T(\tau) \leq z_1^T(\tau)$, a positive response could be obtained through $z_{1,p}$ as a second output, or by including a second controller. Hence, we propose a "dual rail" architecture that combines two controllers in parallel and should improve the performance of the single low-pass controller. To build a dual rail controller (DRC), we connect two sequestration networks in parallel and one in series, and we show that this architecture allows a faster response when compared to a single sequestration module. This idea builds on previous work introducing dual rail molecular circuits [20] and feedback controllers [24], [25] in the context of DNA nanotechnology.

The DRC is sketched in the orange box in Fig. 5B: it includes three sequestration reactions, and two outputs, species X_1 that directly regulates the output Y (like in the single rail controller) and species W, which removes output Y. The first sequestration reaction is identical to the single rail controller and produces X_1 . The second sequestration reaction consists of species X_2 and Z_2 : when compare to the single rail controller, the inputs to this reaction are swapped. The reactions are:

$$R \xrightarrow{\theta_c} Z_2$$
 $Y \xrightarrow{\kappa_c} X_2$ Production $X_2 \xrightarrow{\phi_c} \varnothing$ $Z_2 \xrightarrow{\phi_c} \varnothing$ Decay $X_2 + Z_2 \xrightarrow{\gamma_c} C_2$ Sequestration.

The third sequestration reaction serves as a mechanism to actively produce and remove plant species Y, and includes the reactions:

$$X_1 \xrightarrow{\alpha_s} Y \qquad Y \xrightarrow{\phi_s} \varnothing$$
 Production/Decay
 $X_2 \xrightarrow{\beta_s} W \qquad W \xrightarrow{\phi_s} \varnothing$ Production/Decay
 $Y + W \xrightarrow{\gamma_s} C$ Sequestration

The closed loop system including the dual rail controller is:

$$\dot{x}_1 = \theta_c r - \gamma_c x_1 z_1 - \phi_c x_1,
\dot{z}_1 = \kappa_c y - \gamma_c x_1 z_1 - \phi_c z_1,
\dot{x}_2 = \kappa_c y - \gamma_c x_2 z_2 - \phi_c x_2,
\dot{z}_2 = \theta_c r - \gamma_c x_2 z_2 - \phi_c z_2,
\dot{y} = \alpha_s x_1 - \gamma_c yw - \phi_s y,
\dot{w} = \beta_s x_2 - \gamma_c yw - \phi_s w.$$
(18)

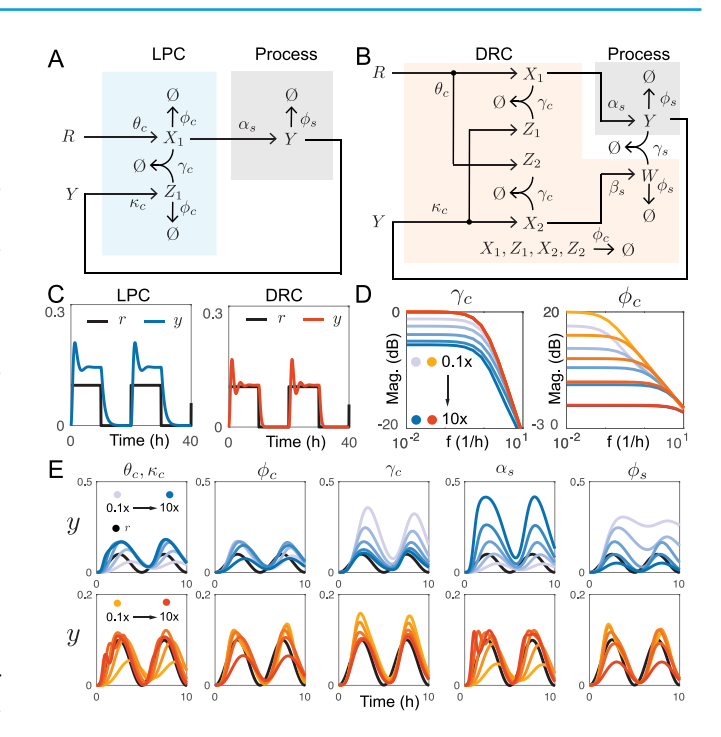


Fig. 5. Simulations comparing controller performance. Reaction schematics of the LPC (A) and DRC (B). (C) Example trajectories under a square wave input. (D) Empirical frequency analysis. (E) Tracking a sinusoidal reference under variation of individual parameters of the controllers ($\theta_C = k_C$, ϕ_C , γ_C) and of the plant (α_S , ϕ_S). The nominal parameters are $\theta_C = k_C = 10$ /h, $\gamma_C = \gamma_S = 10$ / μ M/h, $\alpha_S = \beta_S = \phi_S = \phi_C = 1$ /h.

We omit the dynamics of c_1 (formed by binding of x_1 and z_1), c_2 (formed by x_2 and z_2) and c_3 (formed by y and w).

LPC and DRC performance comparison: Fig. 5C shows example kinetic traces of the LPC and DRC, showing that the LPC tracks the reference with a larger steady state error. This error may due to the presence of dilution $\phi_c \neq 0$ (non-ideal integral controller), or to poor error computation - intended here as the computation of the positive part of the error only. This controller can actively increase y (positive action), while only dilution/degradation can decrease the amount of y. This type of control strategy with just positive action leads to a trade-off between the controller dynamics (that increases y) and the process dynamics (that removes y). When $\phi_c \neq 0$ the gain κ_c/ϕ_c decreases, contributing to a larger steady state error. Even in the presence of dilution, the DRC shows a reduced error presumably because it actively increases and reduces y (using the full error computation).

Fig. 5D shows the "empirical" frequency response of the two controllers as the sequestration rate γ_c or the decay rate ϕ_c are varied. The controller equations in the LPC model (15) and DRC model (18) were fed a periodic input reference $\theta_c r = 0.5(\sin(ft) + 1)/2 + 0.3 \ \mu M/h$, and fixed $\kappa_c y = 0.3 \ \mu M/h$ (we compute the frequency response of the controller in isolation, assuming a constant level of y). We are not able to provide an exact form of the DC gain for the DRC, due to the complexity of its equations.

We then numerically integrated the equations, and measured amplitude and frequency of the output x_1 for the LPC, and the difference of $x_1 - x_2$ (these species deliver opposite actuation on the plant) for the DRC. In these simulations (blue for the

LPC, orange for the DRC) we vary either the sequestration rate γ_c or the decay rate ϕ_c parameter. Both plots resemble the Bode plot of an LPC with a corner frequency near ϕ_c . In the left panel (ϕ_c =1, γ_c varies), the "DC gain" of the DRC does not depend on the sequestration constant γ_c as the LPC. In the right panel, (ϕ_c varies, γ_c = 10) the corner frequency moves as the value of ϕ_c . There is a small offset between the LPC and the DRC, that is inversely proportional to ϕ_c : as ϕ_c decreases, passive down-regulation is reduced and the DRC performs better than the LPC.

Finally, Fig. 5E illustrates the closed loop performance when the reference is a sinusoid, as individual parameters are changed. We assume $\theta_c = \kappa_c$ in all cases. Larger values of $\theta_c = \kappa_c$ improve the tracking performance of both LPC and DRC, however the LPC always shows a significant larger error. Increasing or decreasing ϕ_c in the LPC does not improve its tracking behavior, while for $\phi_c \rightarrow 0$ the DRC shows error reduction. When γ_c is varied, even at small values the DRC maintains better tracking when compared to the LPC. When the plant parameter α_s is perturbed, the DRC confirms to be better at rejecting this disturbance. When changing the plant dilution constant ϕ_s , the DRC performance improves for smaller values, while the LPC performance deteriorates.

VI. CONCLUSION AND DISCUSSION

We have described an approximation of the dynamic behavior of molecular sequestration that illustrates how sequestration computes the difference between input signals.

When compared to previous theoretical work on this topic, our analysis includes dilution/degradation of the reactants (which is always present in living cells) and considers timevarying inputs. The approximation we derived is useful to illustrate how leaky molecular sequestration controllers can be considered low-pass controllers that perform only one side of the subtraction operation. Through simulations, we showed that a dual rail controller (DRC) performs a full subtraction operation, and achieves a lower tracking error across a range of parameters. The DRC requires three sequestration reactions, one of which involves the output Y and species W. In practice, this may be realized through de novo protein switches [26], or σ factors (Y) binding with anti- σ factors (W) driving σ -responsive promoters to express X_2 and Z_1 [18]. The reactants X_i and Z_i (i = 1, 2) may be realized introducing RNA-RNA interactions [16], [17]. We expect that our study will accelerate and generalize the design of biomolecular controllers.

REFERENCES

- N. E. Buchler and F. R. Cross, "Protein sequestration generates a flexible ultrasensitive response in a genetic network," *Mol. Syst. Biol.*, vol. 5, no. 1, p. 272, 2009.
- [2] C. Cosentino, R. Ambrosino, M. Ariola, M. Bilotta, A. Pironti, and F. Amato, "On the realization of an embedded subtractor module for the control of chemical reaction networks," *IEEE Trans. Autom. Control*, vol. 61, no. 11, pp. 3638–3643, Nov. 2016.
- [3] C. Briat, A. Gupta, and M. Khammash, "Antithetic integral feedback ensures robust perfect adaptation in noisy biomolecular networks," *Cell Syst.*, vol. 2, no. 1, pp. 15–26, 2016.

- [4] D. K. Agrawal et al., "Mathematical modeling of RNA-based architectures for closed loop control of gene expression," ACS Synth. Biol., vol. 7, no. 5, pp. 1219–1228, 2018.
- [5] Y. Qian and D. D. Vecchio, "Realizing 'integral control' in living cells: How to overcome leaky integration due to dilution?" *J. Roy. Soc. Interface*, vol. 15, no. 139, 2018, Art. no. 20170902.
- [6] N. Olsman, A.-A. Baetica, F. Xiao, Y. P. Leong, R. M. Murray, and J. C. Doyle, "Hard limits and performance tradeoffs in a class of antithetic integral feedback networks," *Cell Syst.*, vol. 9, no. 1, pp. 49–63, 2019.
- [7] C. C. Samaniego and E. Franco, "A molecular device for frequency doubling enabled by molecular sequestration," in *Proc. IEEE 18th Eur. Control Conf. (ECC)*, 2019, pp. 2146–2151.
- [8] D. Chen and A. P. Arkin, "Sequestration-based bistability enables tuning of the switching boundaries and design of a latch," *Mol. Syst. Biol.*, vol. 8, no. 1, p. 620, 2012.
- [9] X. Ren, C. C. Samaniego, R. M. Murray, and E. Franco, "Bistable state switch enables ultrasensitive feedback control in heterogeneous microbial populations," in *Proc. IEEE Amer. Control Conf. (ACC)*, 2021, pp. 652–659.
- [10] C. C. Samaniego, G. Giordano, and E. Franco, "Practical differentiation using ultrasensitive molecular circuits," in *Proc. 18th Eur. Control Conf.* (ECC), 2019, pp. 692–697.
- [11] C. C. Samaniego, J. Kim, and E. Franco, "Sequestration and delays enable the synthesis of a molecular derivative operator," in *Proc. 59th IEEE Conf. Decis. Control (CDC)*, 2020, pp. 5106–5112.
- [12] A. Moorman, C. C. Samaniego, C. Maley, and R. Weiss, "A dynamical biomolecular neural network," in *Proc. IEEE 58th Conf. Decis. Control* (CDC), 2019, pp. 1797–1802.
- [13] E. Franco, G. Giordano, P.-O. Forsberg, and R. M. Murray, "Negative autoregulation matches production and demand in synthetic transcriptional networks," ACS Synth. Biol., vol. 3, no. 8, pp. 589–599, 2014.
- [14] V. Hsiao, E. L. De Los Santos, W. R. Whitaker, J. E. Dueber, and R. M. Murray, "Design and implementation of a biomolecular concentration tracker," ACS Synth. Biol., vol. 4, no. 2, pp. 150–161, 2015.
- [15] F. Annunziata et al., "An orthogonal multi-input integration system to control gene expression in *Escherichia coli*," ACS Synth. Biol., vol. 6, no. 10, pp. 1816–1824, 2017. [Online]. Available: https://doi.org/10. 1021/acssynbio.7b00109
- [16] H.-H. Huang, Y. Qian, and D. Del Vecchio, "A quasi-integral controller for adaptation of genetic modules to variable ribosome demand," *Nat. Commun.*, vol. 9, no. 1, pp. 1–12, 2018.
- [17] C. L. Kelly, A. W. K. Harris, H. Steel, E. J. Hancock, J. T. Heap, and A. Papachristodoulou, "Synthetic negative feedback circuits using engineered small RNAs," *Nucl. Acids Res.*, vol. 46, no. 18, pp. 9875–9889, 2018. [Online]. Available: https://doi.org/10.1093/nar/gky828
- [18] S. K. Aoki, G. Lillacci, A. Gupta, A. Baumschlager, D. Schweingruber, and M. Khammash, "A universal biomolecular integral feedback controller for robust perfect adaptation," *Nature*, vol. 570, no. 7762, pp. 533–537, 2019.
- [19] H. Steel, A. W. Harris, E. J. Hancock, C. L. Kelly, and A. Papachristodoulou, "Frequency domain analysis of small non-coding rnas shows summing junction-like behaviour," in *Proc. IEEE 56th Annu. Conf. Decis. Control (CDC)*, 2017, pp. 5328–5333.
- [20] K. Oishi and E. Klavins, "Biomolecular implementation of linear I/O systems," *IET Syst. Biol.*, vol. 5, no. 4, pp. 252–260, 2011.
- [21] H. K. Khalil, Nonlinear Systems, 3rd ed. Upper Saddle River, NJ, USA: Prentice-Hall, 2002.
- [22] M. Filo, C.-H. Chang, and M. Khammash, "Biomolecular feedback controllers: From theory to applications," *Current Opin. Biotechnol.*, vol. 79, Feb. 2023, Art. no. 102882.
- [23] C. C. Samaniego and E. Franco, "Ultrasensitive molecular controllers for quasi-integral feedback," *Cell Syst.*, vol. 12, no. 3, pp. 272–288, 2021.
- [24] N. M. Paulino, M. Foo, J. Kim, and D. G. Bates, "PID and state feedback controllers using DNA strand displacement reactions," *IEEE Control* Syst. Lett., vol. 3, no. 4, pp. 805–810, Oct. 2019.
- [25] M. Whitby, L. Cardelli, M. Kwiatkowska, L. Laurenti, M. Tribastone, and M. Tschaikowski, "PID control of biochemical reaction networks," *IEEE Trans. Autom. Control*, vol. 67, no. 2, pp. 1023–1030, Feb. 2022.
- [26] A. H. Ng et al., "Modular and tunable biological feedback control using a de novo protein switch," *Nature*, vol. 572, no. 7768, pp. 265–269, 2019